

Accuracy of the hypothetical sky-polarimetric Viking navigation versus sky conditions: revealing solar elevations and cloudinesses favourable for this navigation method

Dénes Száz^{1,6}, Alexandra Farkas^{1,2,7}, András Barta^{1,3,8}, Balázs Kretzer^{1,9}, Miklós Blahó^{1,10},
Ádám Egri^{1,2,11}, Gyula Szabó^{4,12} and Gábor Horváth^{1,*}

1: ELTE Eötvös Loránd University, Department of Biological Physics, Environmental Optics Laboratory, Pázmány Péter sétány 1, H-1117 Budapest, Hungary

2: MTA Centre for Ecological Research, Danube Research Institute, Karolina út 29-31, H-1113 Budapest, Hungary

3: Estrato Research and Development Ltd, Németvölgyi út 91/c, H-1124 Budapest, Hungary

4: ELTE Eötvös Loránd University, Gothard Astrophysical Observatory, 9700 Szombathely, Szent Imre Herceg utca 112, Hungary

6: e-mail: szaz.denes@gmail.com

7: e-mail: farkas.alexandra@okologia.mta.hu

8: e-mail: bartaandras@gmail.com

9: e-mail: kretzer@caesar.elte.hu

10: e-mail: majkl2000@gmail.com

11: e-mail: egri.adam@okologia.mta.hu

12: e-mail: szgy@gothard.hu

*corresponding author, e-mail: gh@arago.elte.hu

Changes performed along the comments of Referee 1 are marked by violet.

Changes performed along the comments of Referee 2 are marked by green.

Abstract

According to Thorkild Ramskou's theory proposed in 1967, under overcast and foggy skies Viking seafarers might have used skylight polarization analyzed with special crystals called sunstones to determine the position of the invisible Sun. After finding the occluded Sun with sunstones, its elevation angle had to be measured and its shadow had to be projected onto the horizontal surface of a sun-compass. According to Ramskou's theory, these sunstones might have been birefringent calcite or dichroic cordierite or tourmaline crystals working as polarizers. It has frequently been claimed that this method might have been suitable for navigation even in cloudy weather. This hypothesis has been accepted and frequently cited for decades without any experimental support. In this work we determined the accuracy of this hypothetical sky-polarimetric Viking navigation for 1080 different sky situations characterized by solar elevation θ and cloudiness ρ , the sky polarization patterns of which were measured by full-sky imaging polarimetry. We used the earlier measured uncertainty functions of the navigation steps 1, 2 and 3 for calcite, cordierite and tourmaline sunstone crystals and the newly measured uncertainty function of step 4 presented here. As a result, we revealed the meteorological conditions under which Vikings could have used this hypothetical navigation method. We determined the solar elevations at which the navigation uncertainties are minimal at summer solstice and spring equinox for all three sunstone types. On average, calcite sunstone ensures a more accurate sky-polarimetric navigation than tourmaline and cordierite. However, in some special cases (generally at $35^\circ \leq \theta \leq 40^\circ$, $1 \text{ okta} \leq \rho \leq 6 \text{ oktas}$ for summer solstice, and at $20^\circ \leq \theta \leq 25^\circ$, $0 \text{ okta} \leq \rho \leq 4 \text{ oktas}$ for spring equinox) the use of tourmaline and cordierite results in smaller navigation uncertainties than the use of calcite. Generally, under clear or less cloudy skies, the sky-polarimetric navigation is more accurate, but at low solar elevations its accuracy remains relatively large even at high cloudiness. For a given ρ , the absolute value of averaged peak North uncertainties dramatically decreases with increasing θ until the sign (+/-) change of these uncertainties. For a given θ , this absolute value can either decrease or increase with increasing ρ . The most advantageous sky situations for this navigation method are at summer solstice when the solar elevation and cloudiness are $35^\circ \leq \theta \leq 40^\circ$ and $2 \text{ oktas} \leq \rho \leq 3 \text{ oktas}$.

Media Summary

According to Ramskou's theory, under overcast/foggy skies Vikings used skylight polarization analyzed with sunstone crystals to determine the sun position. After finding the occluded Sun, its elevation had to be measured and its shadow had to be projected onto a sun-compass. It has frequently been claimed that this method might have been suitable for navigation even in cloudy weather. Here we determined the accuracy of this hypothetical sky-polarimetric Viking navigation for 1080 different sky situations, the polarization patterns of which were measured by full-sky imaging polarimetry. We revealed the meteorological conditions under which this navigation method can function.

Key words: Viking navigation, sky polarization, sunstone crystal, calcite, cordierite, tourmaline

Introduction

Using easily recognizable coastal places and other simple aids (Sawatzky and Lehn 1976; Thirslund 1997; Kemp and D'Olier 2016), the Vikings discovered new areas between the 9th and 13th century like Iceland, Greenland and the coast of North America. In the North Atlantic region they established colonies that were connected to the European continent through permanent trading routes when the sea-water was free of ice (McGovern 1990; Ingstad and Ingstad 2000; Ogilvie *et al.* 2000). They regularly covered long distances on the ocean lasting several weeks without any modern navigation equipment, such as magnetic compass, for example (May 1955). Solver (1953)

described a navigation method with which the Viking seafarers could have oriented themselves on the open ocean in cloudless weather. His theory is supported by an archeological artefact discovered in 1948, when a fragment of a wooden dial was found under the ruins of a Benedictine convent near the Uunartoq fjord in Greenland (Thirslund 1991). According to the most possible explanations, the dial might have been a fragment of a sun-compass, a navigation tool with which the Viking navigators could determine the geographical North with the help of the shadow of a vertical gnomon cast by the Sun (Solver 1953; Taylor *et al.* 1954; Thirslund 1991, 1993, 1997, 2001). There are, however, alternative explanations for the usage of this device proposed by Bernáth *et al.* (2013a, 2014).

According to the theory of Ramskou (1967) under totally overcast or foggy sky, the Vikings might have used skylight polarization analyzed with special tools called sunstones to determine the position of the invisible Sun. After finding the occluded Sun with sunstones, its elevation angle had to be measured and its shadow had to be projected onto the horizontal surface of a sun-compass. It has been frequently claimed, that this method might also have been suitable for navigation in cloudy weather, even in overcast (Karlsen 2003; Wild and Fromme 2007; Ball 2011). Reference to sunstones can be found in ancient Viking legends, the sagas, being described as tools enabling the determination of the Sun's position behind clouds (Foote 1956; Horváth *et al.* 2014). According to Ramskou's theory, these sunstones might have been birefringent calcite or dichroic cordierite, tourmaline or andalusite minerals (as supposed also by many other researchers: Walker 1978; Schaefer 1997; Karlsen 2003; Wild and Fromme 2007; Ball 2011; Hawthorne and Dirlam 2011; Karman *et al.* 2012; Ropars *et al.* 2012; Le Floch *et al.* 2013; Skalwold and Bassett 2016) that work as polarizers, that is the observer can perceive radiance changes in the skylight coming through. Viking navigators also might have been able to determine the position of the occluded sun with the Haidinger's brushes instead of sunstones (Ropars *et al.* 2012, 2014; Horváth *et al.* 2017).

Ramskou's hypothesis has been accepted and frequently cited for decades without measuring its accuracy under different circumstances. Using imaging polarimetry, we have measured the atmospheric optical prerequisites of the hypothetical sky-polarimetric Viking navigation (Pomozi *et al.* 2001; Suhai and Horváth 2004; Hegedüs *et al.* 2007a,b; Horváth *et al.* 2011; Bernáth *et al.* 2013b, Barta *et al.* 2014). The steps of this navigation method are the followings:

- **1st step:** After calibration of the sunstones in cloudless weather by marking the direction pointing towards the Sun in a well recognizable crystal alignment (e.g. where the radiance of transmitted skylight is minimal or maximal), the Viking navigator might have adjusted the sunstones in cloudy weather at two different celestial points by rotating both in front of his eyes, through which he could determine the directions perpendicular to the local direction of skylight polarization.
- **2nd step:** At this sunstone alignment, the previously carved markings gave the directions of two celestial great circles, in the intersection of which the occluded Sun could be found. The navigator had to determine this intersection by naked eye.
- **3rd step:** Once the position of the Sun was found, the navigator had to measure its vertical elevation with his fists and fingers, in order to reproduce the Sun shadow to use the sun-compass.
- **4th step:** Finally, the shadow-stick of the sun-compass should be aligned parallel to the meridian (vertical azimuth plane) of the invisible Sun.

All four steps have specific uncertainty functions, contributing separately to the North uncertainty $\Delta\omega_N$, the degree with which the estimated northern direction differs from the real geographical North. These uncertainties have been measured in psychophysical laboratory/planetarium experiments, and the accuracy of navigation was calculated assuming that one of these steps was erroneous and the other three steps were accurate (having no uncertainty):

(1) Száz *et al.* (2016a) found that in the 1st step, the sunstone adjustment is more accurate if dichroic tourmaline and cordierite are used when the degree of polarization p of skylight is higher than a critical value p^* (20 % for cordierite and 40 % for tourmaline), while for $p < p^*$ a calcite sunstone can be more accurately adjusted. However, the accuracy of calcite adjustment greatly depends on the crystal quality, because superficial or inner scratches and contamination can disturb or deceive the navigator. (2) Farkas *et al.* (2014) measured the accuracy of intersection estimation of the two great circles in the 2nd step, and found that at lower solar elevations ($5^\circ < \theta < 25^\circ$), the test persons measured the antisolar point instead of the Sun in some cases, resulting in high navigation uncertainty. In the calculation of uncertainty propagation, we removed these measurements of the anti-solar points coming from the second step, thus they did not distort our results. Furthermore, such sun-versus-antisun misestimations might have not been a severe problem in real-life, because the anti-solar point is below the horizon during daytime and if such a spurious mismeasurement occurred (only very sporadically), then the Viking navigators would have likely ignored such wildly discrepant subhorizon solar position estimates using their time sense and the sky brightness (implying also that in the given point of time the sun cannot be under the horizon). Only at sunset and sunrise can the antisun be deceiving, when it is exactly on the horizon, then the Vikings could use their knowledge on the earlier sailing direction (if a navigator used the misestimated antisun instead of the correct sun, the new sailing direction would turn by about 180° relative to the earlier one, and such a too large turn would indicate that a misestimation of the solar position happened). The North uncertainty is also high if the two reference points are far from each other. Thus, the navigation is more accurate around the summer solstice, when the solar elevation is the highest. (3) Száz *et al.* (2016b) measured the accuracy of elevation estimation in the 3rd step. Although both the elevation uncertainty and the North uncertainty increased with solar elevation, 48 % of all elevation estimations were more accurate than $\pm 1^\circ$. (4) In this work we measured the uncertainty function of the 4th step in a planetarium.

Using the uncertainty functions of the four steps of sky-polarimetric navigation (Farkas *et al.* 2014; Száz *et al.* 2016a,b; present work), in this synthesis work we determined the navigation (North) uncertainties under 1080 different meteorological conditions, the sky polarization patterns of which were measured by full-sky imaging polarimetry. These 1080 skies differed in the solar elevation θ and the cloud percent ρ , and were selected from the 1296 different meteorological conditions used by Horváth *et al.* (2017) by omitting the subhorizon cases. The knowledge on sky polarization is reviewed by Können (1985), Coulson (1988), Pomozi *et al.* (2001), Horváth and Varjú (2004), Suhai and Horváth (2004), Hegedüs *et al.* (2007a), Barta *et al.* (2014, 2015) and Horváth *et al.* (2014). The aim of this work is to determine and analyse the accuracy of sky-polarimetric navigation under these many different sky conditions and to answer the most important question of this topic: under what meteorological conditions this hypothetical navigation method could be used? We would like to emphasize that with our study we do not state that we applied the same method as the Vikings did (because nobody knows how the Vikings have really navigated under cloudy and foggy conditions), and we are not trying to prove that the Vikings used this sky-polarimetric navigation. Our aim was to reveal the values of solar elevation and sky cloudiness favourable for this navigation method.

Materials and Methods

Measuring the uncertainty function of the 4th step of sky-polarimetric navigation

In the planetarium of the Eötvös University we measured the uncertainty function of the 4th step of sky-polarimetric navigation. A black dot with angular extension of 0.25° was projected on the white planetarium dome with an azimuth angle φ (ranging between -45° and $+45^\circ$ from an arbitrary horizontal reference direction) and an elevation angle θ (ranging from 0° to 55°). The test person sitting in the center of the planetarium had to estimate the azimuth angle of this dot with the help of a digital goniometer modelling the Viking sun-compass (Supplementary Fig. S1). The person had to

rotate a shadow-stick-shaped elongated metal plate (7 cm long, tilted with 45° from the horizontal) along its vertical axis until its long axis became parallel to the estimated azimuth direction of the projected dot. The difference $\Delta = \varphi_e - \varphi_r$ between the estimated (φ_e) and the true (φ_r) azimuth angles of the dot was registered. The test person had to perform this estimation for 48 dots with random φ - and θ -values. We performed this measurement 10 times with 10 male test persons, whose ages ranged between 23 and 54 years. For a given θ , the resulting $10 \times 10 \times 48 = 4800$ different Δ -values were averaged, thus we obtained the average $\langle \Delta \rangle \pm$ standard deviation (s.d.) σ_φ for 48 different θ -values. Since the average $\langle \Delta \rangle$ -values approximated zero (as expected), the uncertainty function of the 4th step of sky-polarimetric navigation was defined as $e_{4\text{th}}(\theta) = \sigma_\varphi(\theta)$. Finally, a parabola was fitted to the measured $\sigma_\varphi(\theta)$ -values. Further on, this parabola is considered as the uncertainty function of the 4th step.

Selection of 1080 different meteorological situations

The patterns of the degree of polarization p of skylight were measured by imaging polarimetry, the method of which is described in detail by Barta *et al.* (2015). Data on sky polarization have been collected with an automatic full-sky imaging polarimeter set up in the Gothard Astronomical Observatory of the Eötvös University, Szombathely, Hungary ($47^\circ 15' 29.83''$ N, $16^\circ 36' 15.67''$ E). In the last three years this polarimeter functioned continuously and measured several tens of thousands of sky polarization patterns, from which we selected 1080 different skies. We grouped these skies on the basis of the following two parameters: (i) Elevation angle θ of the Sun above the horizon ranged from 0° to 50° (higher solar elevations did not occur at the 61° northern latitude, the main Viking sailing route). This θ -interval was divided into 10 equal intervals with an increment of 5° as follows: $0^\circ \leq \theta_1 < 5^\circ$, $5^\circ \leq \theta_2 < 10^\circ$, $10^\circ \leq \theta_3 < 15^\circ$, $15^\circ \leq \theta_4 < 20^\circ$, $20^\circ \leq \theta_5 < 25^\circ$, $25^\circ \leq \theta_6 < 30^\circ$, $30^\circ \leq \theta_7 < 35^\circ$, $35^\circ \leq \theta_8 < 40^\circ$, $40^\circ \leq \theta_9 < 45^\circ$, $45^\circ \leq \theta_{10} \leq 50^\circ$. (ii) Cloud coverage ρ (% of the full sky covered by clouds) was determined with the use of the cloud detection algorithm k NN (k Nearest Neighbour) described by Barta *et al.* (2015). The interval $0\% \leq \rho \leq 100\%$ was divided into 9 categories, as in meteorology oktas are common units for estimating the cloud coverage of the visible sky region by eyesight (Pasini 2005). Oktas from 0 to 8 refer to more and more intense cloud coverage based on the division of 8 equal intervals (Cazorla *et al.* 2008): okta 0 = totally clear sky, oktas 1-2 = few clouds, oktas 3-4 = scattered clouds, oktas 5-7 = broken clouds, oktas 8 = totally overcast. Based on this generally accepted method, okta 0 corresponds to $\rho_0 = 0\%$, and the further categories are composed of 8 equal intervals with an increment $\Delta\rho = 12.5\%$ as follows: $0\% \leq \rho_1 < 12.5\%$, $12.5\% \leq \rho_2 < 25\%$, $25\% \leq \rho_3 < 37.5\%$, $37.5\% \leq \rho_4 < 50\%$, $50\% \leq \rho_5 < 62.5\%$, $62.5\% \leq \rho_6 < 75\%$, $75\% \leq \rho_7 < 87.5\%$, $87.5\% \leq \rho_8 \leq 100\%$. For example, if the cloud coverage is 3 oktas, this means that approximately 3/8 part of the visible sky is covered by clouds (in our measurement, it falls into the interval $25\% \leq \rho_3 < 37.5\%$). It is not worth, however, separating the totally overcast case ($\rho = 100\%$), because in our measurements all the sky conditions in the 8-okta interval ($87.5\% \leq \rho_8 \leq 100\%$) seemed totally overcast, that could not be separated visually. The cloudless case ($\rho_0 = 0\%$) is easy to recognize, therefore its separation is logical in our measurements. These selected situations were also used by Horváth *et al.* (2017) in a different study.

Beside the cloud coverage ρ , another determinant could be the cloud thickness t . Since our cloud detection algorithm recognized clouds with almost all different t -values, cloud thickness is involved in determinant ρ . Thus, we did not consider t as a separate variable.

Based on the above, we created $10 \times 9 = 90$ (θ , ρ) groups. In each group we selected 12 different skies from our polarimetric sky archives. Finally, we obtained $90 \times 12 = 1080$ different sky situations differing in θ and ρ , but in a given group their θ - and ρ -values were similar. Further on we used the polarization patterns of these skies measured by imaging polarimetry in the green (550 nm) spectral range, in which the human eye is most sensitive (Sharpe *et al.* 2005).

Uncertainty propagation and North uncertainty determination

We determined the navigation uncertainty, that is the North uncertainty $\Delta\omega_N$ for the 1080 different skies supposing that the Viking navigator used one of the three different sunstone crystals: calcite, cordierite or tourmaline. Since in the literature mainly these three crystal types have been assumed to be used as sunstones due to their predominant abundance compared to andalusite, the uncertainty function of the first step of sky-polarimetric navigation has been measured by Száz *et al.* (2016a) only for calcite, cordierite and tourmaline. To quantify the navigation uncertainty, we calculated the uncertainty propagation through the four steps of sky-polarimetric navigation with a custom-made computer program. The basics of this algorithm were used by Száz *et al.* (2016a) for computing the uncertainty propagation in the 1st step of sky-polarimetric navigation. This earlier algorithm was extended and made suitable to calculate the uncertainty propagation when all four navigation steps have their own uncertainty function. $\Delta\omega_N$ was computed with the following algorithm:

- In a given sky, we excluded areas with $p < 5\%$ (being under the sensitivity threshold of the human eye; Száz *et al.* 2016a) and $p > 90\%$ (such high p -values were caused by the motion artefact of clouds and normally do not occur in real skies; Horváth and Varjú 2004; Horváth *et al.* 2014), and pixels of field objects not belonging to the sky.
- We chose point pairs (m_1, m_2) from the non-excluded sky areas as follows: (i) The first point m_1 was chosen from a celestial quadratic grid with a side length of 30 pixels (Fig. 1a). (ii) The second point m_2 was chosen from a celestial polar grid with 20° resolution between angular distances $45^\circ \leq \tau \leq 90^\circ$ from m_1 (Fig. 1b). According to our earlier field experience with sunstones (Bernáth *et al.* 2013b, 2014; Farkas *et al.* 2014), point m_2 cannot be too close to ($0^\circ < \tau < 45^\circ$) or too far ($90^\circ < \tau \leq 180^\circ$) from m_1 , otherwise the accuracy of the 2nd step of sky-polarimetric navigation decreases considerably.
- Using the measured degrees of polarization p_1 and p_2 in sky points m_1 and m_2 , we calculated the uncertainties $e_1 = e(p_1)$ and $e_2 = e(p_2)$ of sunstone adjustment, where $e(p)$ is the uncertainty function of the 1st step measured in psychophysical laboratory experiments for cordierite, tourmaline and (best-performing) calcite crystals (Száz *et al.* 2016a).
- Let C_{1E} and C_{2E} be the great circles passing through the sunstone centers m_1 and m_2 parallel to the straight markings engraved into the sunstone surface during calibration. The estimated Sun position E is the intersection of circles C_{1E} and C_{2E} (Fig. 1c). Let C_{1S} and C_{2S} be the celestial great circles connecting the Sun S with points m_1 and m_2 (Fig. 1d). For each member m_i of the point pair m_1 and m_2 , we considered the two great circles C_{i+} and C_{i-} enclosing an angle of $2e_i(p_i)$ with each other around the great circle C_{iS} connecting points m_i and S , where $i = 1, 2$. C_{i+} and C_{i-} enclose an angle of $+e_i(p_i)$ and $-e_i(p_i)$ with C_{iS} , respectively (Fig. 1d). The intersections of circles C_{1+} , C_{1-} and C_{2+} , C_{2-} appoint a spherical tetragon (marked with grey in Fig. 1d) involving the real Sun position S . Due to the maximum uncertainties $\pm e_i(p_i)$ of sunstone adjustments, all possible estimated Sun positions E are within this grey tetragon for the given point pair m_1 and m_2 . The area of this tetragon was divided into 100 points along a grid with tenth of the tetragon's side length. Thus, we got 100 estimated Sun positions E with which we computed further on. Such trimming of data points was necessary to reduce the computation time of the algorithm.
- To determine the uncertainty of the 2nd navigation step, we characterized the situations with the same four free parameters as Farkas *et al.* (2014): (i) the elevation angle θ_E of the estimated Sun, (ii) γ_1 and (iii) γ_2 meaning the angular distance of m_1 and m_2 from the estimated Sun E , (iv) angle δ enclosed by the planes of the two celestial great circles mentioned. The used parameter intervals were based on the psychophysical planetary experiment of Farkas *et al.* (2014): θ_S : 5° - 25° , 35° - 55° ; γ_1, γ_2 : 35° - 55° , 65° - 85° , 95° - 115° ; δ : 35° - 55° , 65° - 85° , 95° - 115° , 125° - 145° . Thus, we created from these intervals $2 \times 3 \times 3 \times 4 = 72$ parameter groups $(\theta_S, \gamma_1, \gamma_2, \delta)$ and characterized them with the averaged elevation uncertainty $\Delta\theta$ and azimuth uncertainty $\Delta\varphi$ that define a vector $(\Delta\theta, \Delta\varphi)$ in the spherical

coordinate system that mathematically describes the visually spherical sky dome. From the estimated Sun positions E , we selected those that could be sorted into one of the 72 parameter intervals, then these points were shifted with vector $(\Delta\theta, \Delta\varphi)$ on the surface of the hypothetical sky dome (Fig. 1e) in order to add elevation and azimuth uncertainties originating from the 2nd navigation step.

- We determined the vertical elevation of the shifted estimated Sun positions E_{sh} , and calculated the elevation uncertainty $\Delta\theta_E$ based on the uncertainty function of the 3rd step of sky-polarimetric navigation (Száz *et al.* 2016b). For each E_{sh} we got an interval between $E_{sh} - \Delta\theta_E$ and $E_{sh} + \Delta\theta_E$ that was divided into equal vertical angular distances by 0.2° . Thus, instead of one E_{sh} point we got several points based on the elevation uncertainty of the 3rd step, marked with P_θ .
- In the 4th step, the navigator had to align the shadow-stick of the sun-compass parallel to the meridian (vertical azimuth plane) of the invisible Sun. The uncertainty of this alignment was characterized by the measured $e_{4th}(\theta)$ function and for each Sun position P_θ we got an interval between $\varphi_S(\theta) - e_{4th}(\theta)$ and $\varphi_S(\theta) + e_{4th}(\theta)$ that was divided into equal horizontal angular distances by 0.2° perpendicular to the meridian, where $\varphi_S(\theta)$ is the azimuth angle of point P_θ . Thus, instead of each point P_θ , we got several points based on the elevation uncertainty of the 4th step that give the estimated Sun positions P_E , if the uncertainties of all the four steps are calculated in the estimation (Fig. 1g).
- The Viking navigator derived the direction (angle) ω_N of the geographical North using the sun-compass as follows (Fig. 1f): He might have determined the direction of the imaginary light rays originating from position P_E of the invisible Sun with a shadow-stick (Bernáth *et al.* 2013b, 2014). After the horizontal Viking sun compass is rotated until the shadow tip of the vertical gnomon falls on the appropriate gnomonic line engraved in the compass' surface, the symmetry axis of the gnomonic line would exactly point towards the geographical North, if there were no uncertainties. Since in reality the four navigation steps have more or less uncertainties, the symmetry axis of the gnomonic line points towards a direction that differs from the geographical North with an angle ω_N when the shadow tip falls on the gnomonic line. Since the gnomonic line is well visible, we considered the minimal uncertainty of this rotation (which did not affect the navigation) as negligible. This angle ω_N is the navigation uncertainty belonging to (i) a specific pair of sky points m_1 and m_2 with uncertainties e_1 and e_2 of sunstone adjustment in the 1st step, (ii) a parameter group $(\theta_S, \gamma_1, \gamma_2, \delta)$ with elevation and azimuth uncertainties $(\Delta\theta, \Delta\varphi)$ of intersection finding in the 2nd step, (iii) an estimated solar elevation θ_E with elevation uncertainty $\Delta\theta_E$ in the 3rd step, and (iv) an estimated azimuth error of the shadow-stick alignment $e_{4th}(\theta)$ of sky-polarimetric navigation in the fourth step for a given date (e.g. spring equinox, or summer solstice).
- The navigation (or North) uncertainty $\Delta\omega_N$ for a given sky was calculated similarly as in Száz *et al.* (2016a): Angles ω_N for each estimated sun position P_E were collected into a histogram, which were smoothed (convoluted) by a Gaussian function with 5° half-kernel size and 5° standard deviation. This smoothed curve represented the distribution of the North uncertainty $\Delta\omega_N$ with a maximum at angle ω_{max} and a half bandwidth δ_ω meaning the full width at half maximum (Fig. 1h). The smaller the $|\omega_{max}|$ and δ_ω , the more accurate the sky-polarimetric navigation.
- There are always two possibilities to project the estimated sun position P_E onto the gnomonic line (Fig. 1i): either (i) in the forenoon (when the sun-compass is rotated until the shadow tip falls on the forenoon half of the gnomonic line), or (ii) in the afternoon (when the sun-compass is rotated until the shadow tip falls on the afternoon half of the gnomonic line). Thus, we determined the navigation uncertainties $\Delta\omega_N$ for both forenoon and afternoon.

We performed the above calculations (uncertainty propagation) with the use of the uncertainty functions $e(p)$ measured for three different sunstone crystals (calcite, cordierite and tourmaline) for

two astronomically momentous dates (spring equinox and summer solstice, Fig. 1j) and for forenoon and afternoon. This means $3 \times 2 \times 2 = 12 \Delta\omega_N$ data for one sky situation. In all investigated sky situations, we chose only such solar elevations that could have occurred in the onetime Viking habitats at the 61° northern latitude of the main sailing route. Thus, the maximal solar elevation was 29° for spring equinox and 52° for summer solstice (Száz *et al.* 2016a,b). Sky situations above these elevation limits were removed from data evaluation. The gnomonic lines were calculated with the program developed by Bernáth *et al.* (2013a).

Calculation and visualization of data

After computation of uncertainty propagation, we got $12 \times 90 = 1080$ values of North uncertainty $\Delta\omega_N$ for each sunstone crystal at equinox and solstice and for forenoon and afternoon in the 90 (θ , ρ) groups of the selected 1080 sky situations. In Fig. 3 we show the weighted mean

$$\langle \omega_{\max} \rangle = \frac{\sum_{i=1}^N (\omega_{\max})_i (\delta_{\omega})_i^{-2}}{\sum_{i=1}^N (\delta_{\omega})_i^{-2}}, \quad (1)$$

and standard deviation

$$\Delta\omega_{\max} = \frac{\sum_{i=1}^N [(\omega_{\max})_i - \overline{\omega_{\max}}]^2}{N}, \quad \overline{\omega_{\max}} = \frac{\sum_{i=1}^N (\omega_{\max})_i}{N} \quad (2)$$

of peaks ω_{\max} of North uncertainties for each elevation interval marked with rectangles, where $\overline{\omega_{\max}}$ is the arithmetic mean of the ω_{\max} -values in the dataset. The horizontal length of a rectangle is $2\Delta\omega_{\max}$ and the vertical length is uniform. We studied separately navigation in the forenoon and in the afternoon. We also calculated the weighted mean and standard error

$$\delta\omega_{\max} = \sqrt{\frac{1}{\sum_{i=1}^N (\delta_{\omega})_i^{-2}}}, \quad (3)$$

averaged for the 12 values of $\Delta\omega_N$ in the 90 different (θ , ρ) groups. (1)-(3) were calculated for the calcite, cordierite and tourmaline sunstone crystals and for spring equinox and summer solstice. We visualized these data with a matrix in which each cell belongs to a given (θ , ρ) pair and contains the weighed mean $\langle \omega_{\max} \rangle$ of North uncertainties, the values of which are coded with colours (blue and red hues mean negative and positive values, respectively), and in every cell there is a square, the side length of which is proportional to the standard error $\delta\omega_{\max}$ (Figs. 4-6). The data for forenoon and afternoon navigation are visualized separately.

Results

Supplementary Figure S2 shows the average $\langle \Delta \rangle \pm$ standard deviation σ_{ϕ} of the difference $\Delta = \phi_e - \phi_r$ between the estimated (ϕ_e) and the real (ϕ_r) azimuth angles of dots projected on a dome as a function of the elevation angle θ of the dots measured psychophysically in a planetarium on 10 test persons 10-times. Figure 2 represents the uncertainty function $e_{4\text{th}}(\theta) = 0.0002 \cdot \theta^2 + 1.1829$ of the 4th step of sky-polarimetric navigation fitted to the measured $\sigma_{\phi}(\theta)$ -values.

According to Fig. 3 (Supplementary Tables S1-S3), we can see that at summer solstice the smallest North uncertainties occur at solar elevation $35^\circ \leq \theta \leq 40^\circ$ (with $|\langle \omega_{\max} \rangle| = 3.4^\circ$ for calcite in the forenoon and $|\langle \omega_{\max} \rangle| = 1.8^\circ$ in the afternoon, $|\langle \omega_{\max} \rangle| = 2.9^\circ$ for cordierite in the forenoon and $|\langle \omega_{\max} \rangle| = 1.6^\circ$ in the afternoon, $|\langle \omega_{\max} \rangle| = 1.2^\circ$ for tourmaline in the forenoon and $|\langle \omega_{\max} \rangle| = 0.2^\circ$ in the afternoon). At spring equinox, the smallest North uncertainties occur for solar elevations $15^\circ \leq \theta \leq 25^\circ$ (with $|\langle \omega_{\max} \rangle| = 6.2^\circ$ for calcite in the forenoon and $|\langle \omega_{\max} \rangle| = 3.7^\circ$ in the afternoon, $|\langle \omega_{\max} \rangle| = 7.1^\circ$ for cordierite in the forenoon and $|\langle \omega_{\max} \rangle| = 3.0^\circ$ in the afternoon, $|\langle \omega_{\max} \rangle| = 5.4^\circ$ for tourmaline in the forenoon and $|\langle \omega_{\max} \rangle| = 6.3^\circ$ in the afternoon).

Using any of the three investigated sunstone crystals, at summer solstice the standard deviation $\Delta\omega_{\max}$ of peaks ω_{\max} of North uncertainties decreases with increasing solar elevation θ both for the forenoon and the afternoon navigation if $\theta < 35^\circ$, then $\Delta\omega_{\max}$ increases strongly with increasing θ (Fig. 3). At spring equinox, however, $\Delta\omega_{\max}$ tentatively increases with increasing θ for all three sunstones in the forenoon as well as in the afternoon (Fig. 3).

The North uncertainties both in the forenoon and the afternoon change sign (+/-) at $40^\circ \leq \theta \leq 45^\circ$ at summer solstice and at $20^\circ \leq \theta \leq 25^\circ$ at spring equinox (Fig. 3). The same effect occurs at spring equinox as well, though then the maximal solar elevation is lower.

Comparing the three sunstone crystals (Fig. 3, Supplementary Tables S1-S3), at spring equinox for solar elevations $\theta \leq 20^\circ$, the smallest standard deviations $\Delta\omega_{\max}$ of peaks ω_{\max} of North uncertainties occur for calcite ($2.2^\circ < \Delta\omega_{\max} < 4.3^\circ$), the largest $\Delta\omega_{\max}$ -values are for tourmaline ($2.5^\circ < \Delta\omega_{\max} < 5.3^\circ$) and the $\Delta\omega_{\max}$ -values of cordierite are in-between ($2.1^\circ < \Delta\omega_{\max} < 5.2^\circ$). At summer solstice for solar elevations $\theta \leq 35^\circ$, the smallest standard deviations $\Delta\omega_{\max}$ of peaks ω_{\max} of North uncertainties occur for calcite ($1.1^\circ < \Delta\omega_{\max} < 4.5^\circ$), the largest $\Delta\omega_{\max}$ -values are for tourmaline ($2.1^\circ < \Delta\omega_{\max} < 7.3^\circ$) and the $\Delta\omega_{\max}$ -values of cordierite are in-between ($1.4^\circ < \Delta\omega_{\max} < 5.8^\circ$).

Figures 4-6 (Supplementary Tables S4-S6) show the weighted mean $\langle \omega_{\max} \rangle$ and standard error $\delta\omega_{\max}$ of peaks ω_{\max} of North uncertainties for different sky situations characterized by the groups of solar elevation θ and cloudiness ρ :

- **At summer solstice** the most accurate navigation is at $35^\circ \leq \theta \leq 40^\circ$ in the case of all three sunstone crystals (Figs. 4-6). Then, the most accurate navigation with minimal absolute weighted mean $|\langle \omega_{\max} \rangle|$ ($\langle \omega_{\max} \rangle = -1.4^\circ$) is at $\rho = 2$ and 7 oktas in the forenoon and at $\rho = 7$ oktas ($\langle \omega_{\max} \rangle = -0.1^\circ$) in the afternoon for calcite (Fig. 4), at $\rho = 7$ oktas ($\langle \omega_{\max} \rangle = -0.4^\circ$) in the forenoon and at $\rho = 2$ oktas ($\langle \omega_{\max} \rangle = 0.0^\circ$) in the afternoon for cordierite (Fig. 5), at $\rho = 3$ oktas ($\langle \omega_{\max} \rangle = -0.2^\circ$) in the forenoon and at $\rho = 3$ oktas ($\langle \omega_{\max} \rangle = 0.3^\circ$) in the afternoon for tourmaline (Fig. 6).
- **At spring equinox** the minimum $|\langle \omega_{\max} \rangle|$ -values are at $15^\circ \leq \theta \leq 20^\circ$, $\rho = 8$ oktas ($\langle \omega_{\max} \rangle = -0.2^\circ$) in the forenoon and at $20^\circ \leq \theta \leq 25^\circ$, $\rho = 1$ okta ($\langle \omega_{\max} \rangle = -0.4^\circ$) in the afternoon for calcite (Fig. 4), at $15^\circ \leq \theta \leq 20^\circ$, $\rho = 8$ oktas ($\langle \omega_{\max} \rangle = 0.1^\circ$) in the forenoon and at $20^\circ \leq \theta \leq 25^\circ$, $\rho = 0$ okta ($\langle \omega_{\max} \rangle = -0.1^\circ$) in the afternoon for cordierite (Fig. 5), and at $15^\circ \leq \theta \leq 20^\circ$, $\rho = 8$ oktas ($\langle \omega_{\max} \rangle = 0.9^\circ$) in the forenoon and at $20^\circ \leq \theta \leq 25^\circ$, $\rho = 1$ okta ($\langle \omega_{\max} \rangle = -1.1^\circ$) in the afternoon for tourmaline (Fig. 6). For a given ρ , the absolute value of $\langle \omega_{\max} \rangle$ dramatically decreases with increasing θ until the sign (+/-) change of $\langle \omega_{\max} \rangle$ -values. For a given θ , this absolute value can either decrease or increase with increasing ρ , meaning that there is no strong dependence on the cloud coverage ρ (Figs. 4-6).

The most unsuitable meteorological situations for sky-polarimetric navigation are the following (Figs. 4-6):

- (i) High solar elevations: $45^\circ \leq \theta \leq 50^\circ$ when $27^\circ \leq |\langle \omega_{\max} \rangle|_{\text{calcite}} \leq 47^\circ$ (Fig. 4), $23^\circ \leq |\langle \omega_{\max} \rangle|_{\text{cordierite}} \leq 47^\circ$ (Fig. 5), $26^\circ \leq |\langle \omega_{\max} \rangle|_{\text{tourmaline}} \leq 51^\circ$ (Fig. 6). These elevation values occur only at summer solstice.
- (ii) Low solar elevations with high cloudiness: $0^\circ \leq \theta \leq 10^\circ$, $5 \text{ oktas} \leq \rho \leq 8 \text{ oktas}$. Then, the

weighted mean of navigation uncertainties are $21^\circ \leq |\langle \omega_{\max} \rangle|_{\text{calcite}} \leq 38^\circ$ (Fig. 4), $21^\circ \leq |\langle \omega_{\max} \rangle|_{\text{cordierite}} \leq 39^\circ$ (Fig. 5), $22^\circ \leq |\langle \omega_{\max} \rangle|_{\text{tourmaline}} \leq 44^\circ$ (Fig. 6).

Discussion

The longitude could probably not have been determined by the Vikings, because this requires the availability of accurate clocks. The purpose of the Viking sun compass was to determine a specific reference direction (such as the North or the West), rather than the longitude. However, using this instrument, the longitude and local noon could also have been determined as Bernáth *et al.* (2013a) alternatively interpreted the Viking sundial artefact. Although Bernáth *et al.* (2014) have also shown that the Uunartoq artefact fragment could also have been used before sunrise and after sunset, in this work we followed the original theory about the application of the device as a sun-compass. Here we determined the accuracy of sky-polarimetric navigation with the use of the earlier measured uncertainty functions of the four navigation steps for birefringent calcite and dichroic cordierite and tourmaline sunstone crystals (Farkas *et al.* 2014; Száz *et al.* 2016a,b) for 1080 different sky situations characterized by the solar elevation θ and cloudiness ρ . We obtained that both in the forenoon and the afternoon and for all three sunstones, at spring equinox the standard deviation of North uncertainty peaks $\Delta\omega_{\max}$ tendentially increases with increasing θ , while at summer solstice the standard deviation $\Delta\omega_{\max}$ of peaks ω_{\max} of North uncertainties decreases with increasing solar elevation θ if $\theta < 35^\circ$, then $\Delta\omega_{\max}$ increases strongly with increasing θ (Fig. 3). The reason for these is the complex interaction of the θ -dependent uncertainty functions of the four steps of sky-polarimetric navigation during the uncertainty propagation.

The net North uncertainty is the result of a complex propagation of the uncertainties of the four navigation steps. The uncertainties from the 1st step contribute considerably to the net navigation uncertainty if the degree of polarization p of skylight is low. The uncertainties of the 2nd step are the most dominant at low solar elevations ($\theta < 35^\circ$ for summer solstice, and $\theta < 20^\circ$ for spring equinox) and the uncertainties of the 3rd step become dominant at high solar elevations. The 4th step (the error of which is always $< 2.5^\circ$) has only a slight contribution to the net North uncertainty which is the largest for the highest solar elevations $\theta > 45^\circ$ at summer solstice (Fig. 2).

With low cloudiness the direct sun could frequently be used for Viking navigation. Even with high cloud cover, the sky radiation and polarization are variable. To a given cloudiness infinite cloud patterns can belong, in many of which the sun is visible. However, in our 1080 carefully selected cloudy skies the sun was occluded by clouds, furthermore, we selected 12 different skies with invisible sun for a given ρ - θ cell. Thus, although using oktas for the description of the celestial cloud cover is far from being complete, the 1080 different sky situations are enough to model the variability of the cloudy sky with which Viking navigators had to cope.

The sign change of the North uncertainty both in the forenoon and the afternoon (Fig. 3) can partly be explained with the characteristics of the elevation uncertainty in the 3rd step of sky-polarimetric navigation: The contribution of underestimating solar elevation increases with increasing θ (Száz *et al.* 2016b), thus, the North uncertainties are shifted in the opposite direction. At lower solar elevations, the navigator can practically only overestimate the elevation θ , because underestimations would cause the Sun positioned below the horizon that did not occur in our situations. In such cases (at lower solar elevations), there is no gnomon shadow that could have reached the gnomonic line on the horizontal surface of the sun-compass. However, elevation uncertainties for low solar elevations are much smaller than for high elevations (Száz *et al.* 2016b).

The 3rd step uncertainty cannot alone explain the sign change. The net uncertainty of the 2nd navigation step (Farkas *et al.* 2014, Supplementary Table S7) also has an elevation uncertainty component which is rather large ($|\Delta\theta| < 21^\circ$) for low solar elevations ($5^\circ \leq \theta \leq 25^\circ$) and is dominantly positive, meaning overestimations, while for high elevations ($35^\circ \leq \theta \leq 55^\circ$) these uncertainties are small ($|\Delta\theta| < 6^\circ$) and in approximately equal number positive and negative which does not have a significant contribution to the resulting elevation uncertainty. At higher θ -values, as θ increases the overestimations of the solar elevation become less dominant, and for $35^\circ \leq \theta \leq 40^\circ$

at summer solstice and for $20^\circ \leq \theta \leq 25^\circ$ at spring equinox over- and underestimations of θ occur with similar frequency. At high solar elevations around the daily maximum of θ , dominantly underestimations of θ can occur, because if the estimated Sun were above the possible daily maximum, the tip of the gnomon shadow could not reach the gnomonic line. In such cases, the Viking navigator had to re-measure the solar elevation, because he could not use it for North estimation. These underestimated solar elevations around noon give North uncertainties with the opposite sign relative to the overestimated elevations around sunset or sunrise. In Fig. 3 it is also clearly seen that logically, the sign of North uncertainties in the forenoon is the opposite of the sign in the afternoon, because the sun-compass has to be rotated in the opposite direction so that the shadow tip can reach the gnomonic line.

We obtained that sky-polarimetric navigation is most accurate for solar elevations $35^\circ \leq \theta \leq 40^\circ$ at summer solstice and for $15^\circ \leq \theta \leq 25^\circ$ at spring equinox (Figs. 4-6). It is remarkable that the majority of the less overcast situations were the most suitable (possessing the smallest North uncertainties) for sky-polarimetric navigation at a given solar elevation. However, we cannot exclude the possibility that this navigation method was also usable in strong cloudy circumstances, because in some sky situations the minimum of the weighted mean $|\langle \omega_{\max} \rangle|$ of North uncertainties is at cloudiness $\rho = 7-8$ oktas. We found that the most advantageous sky situations for this navigation method are at summer solstice when the solar elevation and cloudiness are $35^\circ \leq \theta \leq 40^\circ$ and $1 \text{ okta} \leq \rho \leq 7$ oktas. Although there is no archaeological evidence of increased Viking seafaring during summertime (near summer solstice) as opposed to springtime (near spring equinox), our findings show that in summer the sky-polarimetric navigation is more accurate than in spring.

The sky situations being the most unsuitable for sky-polarimetric navigation (i.e. having the largest North uncertainties) are more obvious: These are generally when the solar elevation is low ($0^\circ \leq \theta \leq 10^\circ$) and the cloudiness is high ($\rho = 5-8$ oktas) when the orientation uncertainties are the highest for all three sunstone crystals and both for summer solstice and spring equinox. At summer solstice, very high solar elevations ($45^\circ \leq \theta \leq 50^\circ$) can also be disadvantageous due to the high North uncertainties.

If the navigator measured and corrected his orientation several times a day with equal temporal distribution in the forenoon and the afternoon, the North uncertainties averaged for the whole day should be relatively small due to the opposite sign of forenoon and afternoon North uncertainties (Figs. 3-6). This is in accordance with the earlier findings (Thirslund 2001) that in sunshine (when the Viking sun-compass is easy to use in direct sunlight) it was worth for the Vikings orienting themselves regularly, several times a day during their sailing routes.

Further uncertainties are introduced due to the different qualities of sunstones. Száz *et al.* (2016a) studied four calcite crystals of different qualities. In this work, we used the uncertainty function of the best calcite. Comparing the different sunstone crystal types, the use of birefringent calcite results in a more accurate sky-polarimetric navigation on average, because the weighted mean and standard error of North uncertainties are smaller than those for dichroic tourmaline and cordierite crystals. However, in some special sky situations (generally at $35^\circ \leq \theta \leq 40^\circ$, $1 \text{ okta} \leq \rho \leq 6$ oktas for summer solstice, and at $20^\circ \leq \theta \leq 25^\circ$, $0 \text{ okta} \leq \rho \leq 4$ oktas for spring equinox), tourmaline and cordierite crystals performed better, respectively, resulting in smaller North uncertainties, that is a more accurate navigation. The extraordinary performance of the calcite sunstone used in this work can be explained by the fact that we selected the best-performing calcite crystal from the four different calcites used in our former psychophysical laboratory experiment (Száz *et al.* 2016a). Although this was a special choice, it is pertinent to suppose that Viking navigators might also have selected the best-performing calcite crystals from the available ones. If one crystal worked poorly during their journey (resulting in an inaccurate navigation), they could choose another one for their next journey, or, in the worst case, only those seafarers survived who had the best sunstones for navigation.

Most of the studies on Viking navigation (Ramskou 1967; Schaefer 1997; Karlsen 2003; Ball 2011; Hawthorne and Dirlam 2011; Karman *et al.* 2012) mentioned calcite crystals as the alleged Viking sunstones, without any quantitative measurements to prove their assumption. If a

calcite crystal is ideal, having no contamination and crystal defects, it results in a more accurate navigation, because the two spots/slots seen through it due to double refraction ensure differential analysis of sky polarization, which is inherently more accurate than analyzing polarization on the basis of the temporal sinusoid change of radiance of light transmitted through a rotating dichroic tourmaline or cordierite crystal. However, Száz *et al.* (2016a) showed that the adjustment uncertainties of calcite crystals with contamination and crystal defects can be larger than those of tourmaline and cordierite. Our results presented here corroborate experimentally the widespread belief that calcite can be a better sunstone than tourmaline and cordierite. But we conclude, that calcite is advised to use as sunstone under general sky conditions. In the above-mentioned special sky situations (generally at $35^\circ \leq \theta \leq 40^\circ$, $1 \text{ okta} \leq \rho \leq 6 \text{ oktas}$ for summer solstice, and at $20^\circ \leq \theta \leq 25^\circ$, $0 \text{ okta} \leq \rho \leq 4 \text{ oktas}$ for spring equinox), it is worth choosing cordierite or tourmaline instead.

We interestingly found that a 61° North latitude sailing route may not have been as severe a hindrance to sky-polarimetric navigation as one would naively have thought, since north uncertainties dramatically increase for solar elevations $\theta > 40^\circ$. Since the navigation uncertainty tendenciously increases with increasing θ , a navigator based on the Equator with much larger θ -values may have had quite a difficult time using this technique. Finally, we admit that in our studies (psychophysical laboratory and planetarium experiments) the circumstances were ideal. In a real-life situation, the continuous swaying and rolling of the ship, blowing and cold weather necessarily affect the accuracy of sky-polarimetric navigation. These real circumstances would have been a major handicap to align, for example, the shadow-stick or to accurately position the sunstones. Narrow vessels like those the Vikings used are prone to rocking and bobbing even in smooth seas, but can somewhat be stabilized by hoisting a sail. Thus, our results obviously underestimate the real-life North uncertainties of this navigation method.

Originally and most frequently, Vikings had determined the North (West-East) direction. Sometimes they had to know the actual latitude. If the latter differed considerably from 61° , then they had to compensate this by addition or subtraction of an angle to/from the North (West-East) direction. These are two different navigation tasks. The determination of the ideal frequency of the former task is the subject of a further study, the results of which will be published in a separate paper.

Although at **nighttime** the polar star could also have been used, in the time of Vikings the Polar star (Polaris) was positioned much farther from the **celestial** North Pole. Thus Vikings could not have used it for accurate navigation.

This work deals with the solar elevations and cloudinesses favourable for the hypothetical sky-polarimetric Viking navigation. **Using the results presented in this work, we plan to quantify** the maximum navigation error that allows successful navigation meaning that voyages can reach the Viking settlement Hvarf in south Greenland from the Norwegian Hernam (now Bergen) along the 61° northern latitude, their main sailing route between Norway and Greenland. After such a computer simulation of the voyages we can reveal how many degrees of navigation error throughout a voyage are acceptable. This could potentially be 1) an estimate of the latitudinal discrepancy resulting from a longitudinal voyage given 2) a random walk of the azimuthal heading when exposed to the averaged peak North uncertainties and 3) some average, representative skies across the duration of the voyage. The results of such a planned investigation will demonstrate i) how close to the planned disembarkation location a navigator could achieve, ii) at what time of year and weather conditions is polarimetric navigation of highest and lowest quality, iii) which sunstone type (calcite, cordierite or tourmaline) is the most favourable for this navigation, and iv) would polarimetric navigation truly have been a viable method of navigation for Viking seafarers.

Data accessibility

All supporting data of our studies are made available as supplementary information of this paper.

Competing interests

We state that we have no competing interests.

Authors' contributions

- 1) Substantial contributions to conception and design: GH, AF, DS
- 2) Performing experiments and data acquisition: GH, AF, DS, GS, AB, BK, MB, ÁE
- 3) Data analysis and interpretation: GH, DS
- 4) Drafting the article or revising it critically for important intellectual content: GH, AF, DS
- 5) All authors gave final approval for publication.

Acknowledgements

We are grateful to Prof. Kristóf Petrovay (head of the Department of Astronomy) for permitting our psychophysical measurements in the planetarium of the Eötvös University. We thank Dóra Nehéz and Anita Strifler for their logistical help in the planetarium. We thank the 10 test persons for their participation in our planetarium measurements. We thank the constructive and valuable comments of two anonymous reviewers.

Funding statement

This work was supported by the grant OTKA K-105054 (Full-Sky Imaging Polarimetry to Detect Clouds and to Study the Meteorological Conditions Favourable for Polarimetric Viking Navigation) received by Gábor Horváth from the Hungarian Science Foundation. G. S. thanks for the grant GINOP-2.3.2-15-2016-00003 obtained from the Hungarian National Research, Development and Innovation Office (NKFIH).

Ethics statement

For our studies no permission, licence or approval was necessary.

References

- Ball P. (2011) Material witness: a light compass? *Nature Materials* 10: 814 (doi:10.1038/nmat3153)
- Barta A., Farkas A., Száz D., Egri Á., Barta P., Kovács J., Csák B., Jankovics I., Szabó G., Horváth G. (2014) Polarization transition between sunlit and moonlit skies with possible implications for animal orientation and Viking navigation: anomalous celestial twilight polarization at partial moon. *Applied Optics* 53: 5193-5204
- Barta A., Horváth G., Horváth Á., Egri Á., Blahó M., Barta P., Bumke K., Macke A. (2015) Testing a polarimetric cloud imager aboard research vessel polarstern: comparison of color-based and polarimetric cloud detection algorithms. *Applied Optics* 54: 1065-1077
- Bernáth B., Blahó M., Egri Á., Barta A., Horváth G. (2013a) An alternative interpretation of the Viking sundial artefact: an instrument to determine latitude and local noon. *Proceedings of the Royal Society A* 469: 20130021 (doi:10.1098/rspa.2013.0021)
- Bernáth B., Blahó M., Egri Á., Barta A., Kriska G., Horváth G. (2013b) Orientation with a Viking sun-compass, a shadow-stick, and two calcite sunstones under various weather conditions. *Applied Optics* 52: 6185-6194
- Bernáth B., Farkas A., Száz D., Blahó M., Egri Á., Barta A., Åkesson S., Horváth G. (2014) How could the Viking Sun compass be used with sunstones before and after sunset? Twilight board as a new interpretation of the Unartoq artefact fragment. *Proceedings of the Royal Society A* 470: 20130787 (doi:10.1098/rspa.2013.0787)

- Cazorla A., Olmo F. J., Alados-Arboledas L. (2008) Development of a sky imager for cloud cover assessment. *Journal of the Optical Society of America A* 25: 29-39
- Coulson K. L. (1988) *Polarization and Intensity of Light in the Atmosphere*. A. Deepak Publishing, Hampton, Virginia, USA
- Farkas A., Száz D., Egri Á., Blahó M., Barta A., Nehéz D., Bernáth B., Horváth G. (2014) Accuracy of sun localization in the second step of sky-polarimetric Viking navigation for north determination: a planetarium experiment. *Journal of the Optical Society of America A* 31: 1645-1656
- Foote P. G. (1956) Icelandic sólarsteinn and the Medieval Background. *Arv. J. Scand. Folklore* 12: 26-40
- Hawthorne C. F., Dirlam D.M. (2011) Tourmaline the indicator mineral: from atomic arrangement to Viking navigation. *Elements* 7: 307-312
- Hegedüs R., Åkesson S., Horváth G. (2007a) Polarization patterns of thick clouds: overcast skies have distribution of the angle of polarization similar to that of clear skies. *Journal of the Optical Society of America A* 24: 2347-2356
- Hegedüs R., Åkesson S., Wehner R., Horváth G. (2007) Could Vikings have navigated under foggy and cloudy conditions by skylight polarization? On the atmospheric optical prerequisites of polarimetric Viking navigation under foggy and cloudy skies. *Proceedings of the Royal Society A* 463: 1081-1095
- Horváth G., Takács P., Kretzer B., Szilasi S., Száz D., Farkas A., Barta A. (2017) Celestial polarization patterns sufficient for Viking navigation with the naked eye: Detectability of Haidinger's brushes on the sky versus meteorological conditions. *Royal Society Open Science* 4: 160688 (doi: 10.1098/rsos.160688)
- Horváth G., Barta A., Hegedüs R. (2014) Chapter 18: Polarization of the sky. pp. 367-406. In: G. Horváth (editor) (2014) *Polarized Light and Polarization Vision in Animal Sciences*. Springer: Heidelberg, Berlin, New York
- Horváth G., Varjú D. (2004) *Polarized Light in Animal Vision - Polarization Patterns in Nature*. Springer: Heidelberg, Berlin, New York
- Horváth G., Barta A., Pomozi I., Suhai B., Hegedüs R., Åkesson S., Meyer-Rochow B., Wehner R. (2011) On the trail of Vikings with polarized skylight: experimental study of the atmospheric optical prerequisites allowing polarimetric navigation by Viking seafarers. *Philosophical Transactions of the Royal Society B* 366: 772-782
- Horváth G., Farkas A., Bernáth B. (2014) Chapter 25: Sky-polarimetric Viking navigation. pp. 603-635. In: G. Horváth (editor) (2014) *Polarized Light and Polarization Vision in Animal Sciences*. Springer: Heidelberg, Berlin, New York
- Ingstad H., Ingstad A. S. (2000) *The Viking Discovery of America. The Excavation of a Norse Settlement in L'Anse aux Meadows*. Breakwater Book Ltd., Newfoundland. St. John's., Canada
- Karman S. B., Diah S. Z. M., Gebeshuber I. C. (2012) Bio-inspired polarized skylight-based navigation sensors: a review. *Sensors* 12: 14232-14261
- Karlsen L. K. (2003) *Secrets of the Viking Navigators*. One Earth Press: Seattle, USA
- Kemp J., D'Olier B. (2016) Early navigation in the North Sea: the use of the lead and line and other navigation methods. *Journal of Navigation* 69: 673-697
- Können G. P. (1985) *Polarized Light in Nature*. Cambridge University Press, Cambridge
- Le Floch A., Ropars G., Lucas J., Wright S., Davenport T., Corfield M., Harrisson M. (2013) The sixteenth century Alderney crystal: a calcite as an efficient reference optical compass? *Proceedings of the Royal Society A* 469: 20120651 (doi:10.1098/rspa.2012.0651)
- May, W. E. (1955) Alexander Neckham and the pivoted compass needle. *Journal of Navigation* 8: 283-284
- McGovern T. H. (1990) The archaeology of the Norse North Atlantic. *Annual Review of Anthropology* 19: 331-351
- Ogilvie A. E. J., Barlow L. K., Jennings A. E. (2000) North Atlantic climate c. ad. 1000: Millennial

- reflections on the Viking discoveries of Iceland, Greenland and North America. *Weather* 55: 34-45
- Pasini A. (2005) From Observations to Simulations. A Conceptual Introduction to Weather and Climate Modelling. *World Scientific Publishing Co. Pte. Ltd.* Mainland Press: Singapore
- Pomozi I., Horváth G., Wehner R. (2001) How the clear-sky angle of polarization pattern continues underneath clouds: full-sky measurements and implications for animal orientation. *Journal of Experimental Biology* 204: 2933-2942
- Ramskou T. (1967) Solstenen. *Skalk* 2: 16-17
- Ropars G., Gorre G., Le Floch A., Enoch J., Lakshminarayanan V. (2012) A depolarizer as a possible precise sunstone for Viking navigation by polarized skylight. *Proceedings of the Royal Society A* 468: 671-684
- Ropars G., Lakshminarayanan V., Le Floch A. (2014) The sunstone and polarised skylight: ancient Viking navigational tools? *Contemporary Physics* 55: 302-317
- Sawatzky H. L., Lehn W. H. (1976) The Arctic mirage and the early North Atlantic. *Science* 192: 1300-1305
- Schaefer B. E. (1997) Vikings and polarization sundials. *Sky and Telescope* 93: 91-94
- Sharpe L. T., Stockman A., Jagla W., Jagle H. (2005) A luminous efficiency function, $V^*(\lambda)$, for daylight adaptation. *Journal of Vision* 5: 948-968
- Skalwold E. A., Bassett W. A. (2016) Blue minerals: exploring cause and effect. *Rocks and Minerals* 91: 61-77
- Solver C. V. (1953) The discovery of an early bearing-dial. *Journal of Navigation* 6: 294-296
- Suhai B., Horváth G. (2004) How well does the Rayleigh model describe the E-vector distribution of skylight in clear and cloudy conditions? A full-sky polarimetric study. *Journal of the Optical Society of America A* 21: 1669-1676
- Száz D., Farkas A., Blahó M., Barta A., Egri Á., Kretzer B., Hegedüs T., Jäger Z., Horváth G. (2016a) Adjustment errors of sunstones in the first step of sky-polarimetric Viking navigation: studies with dichroic cordierite/tourmaline and birefringent calcite crystals. *Royal Society Open Science* 3: 150406 (doi:10.1098/rsos.150406)
- Száz D., Farkas A., Barta A., Kretzer B., Egri Á., Horváth G. (2016b) North error estimation based on solar elevation errors in the third step of sky-polarimetric Viking navigation. *Proceedings of the Royal Society A* 472: 20160171 (doi: 10.1098/rspa.2016.0171)
- Taylor E. G., May W. E., Motzo R. B., Lethbridge T. C. (1954) A Norse bearing-dial? *Journal of Navigation* 7: 78-84
- Thirslund S. (1991) A presumed sun compass from Narsarsuaq. In The church topography of the eastern settlement and the excavation of the Benedictine convent at Narsarsuaq in the Uunartoq Fjord (ed. C. L. Vebæk), pp. 65-71. *Monographs on Greenland* vol. 278: *Man & Society*, vol. 14. Copenhagen, Denmark: Museum Tusulanum Press
- Thirslund S. (1993) The discovery of an early bearing-dial - Further investigations. *Journal of Navigation* 46: 33-48
- Thirslund S. (1997) Sailing directions of the North Atlantic Viking age (from about the year 860 to 1400). *Journal of Navigation* 50: 55-64
- Thirslund S. (2001) *Viking Navigation. Sun-compass guided Norsemen first to America*. Humlebæk. Denmark: Gullanders Bogtrykkeri a-s, Skjern
- Walker J. (1978) The amateur scientist: More about polarizers and how to use them, particularly for studying polarized sky light. *Scientific American* 238 (1): 132-136
- Wild W., Fromme B. (2007) Der Sonnenstein der Wikinger: Navigation mit polarisiertem Himmelsicht. *Praxis der Naturwissenschaften - Physik in der Schule* 56: 33-38

Figures with Legends

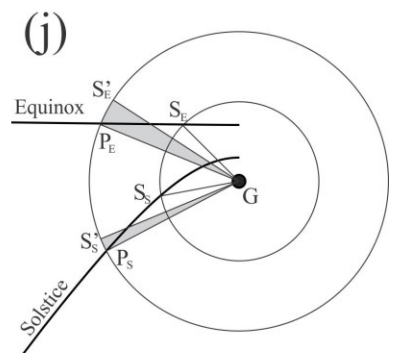
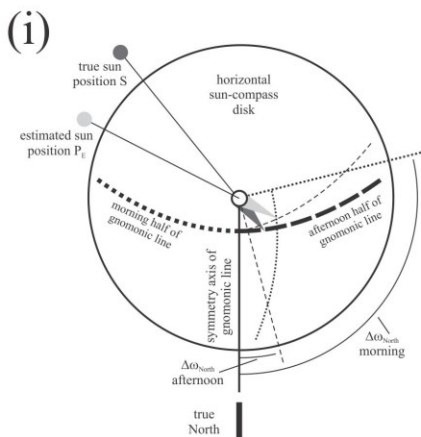
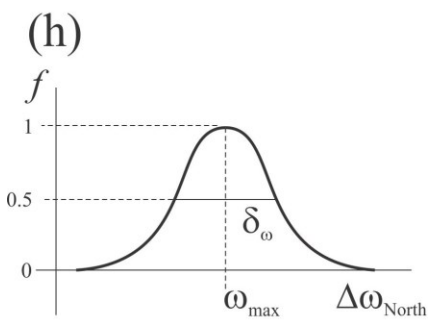
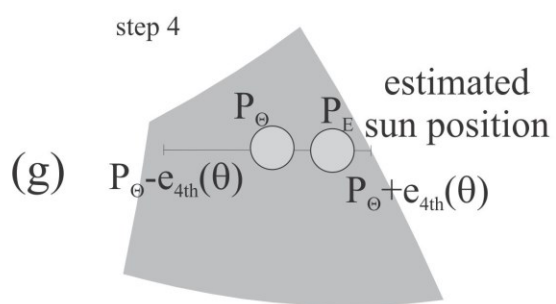
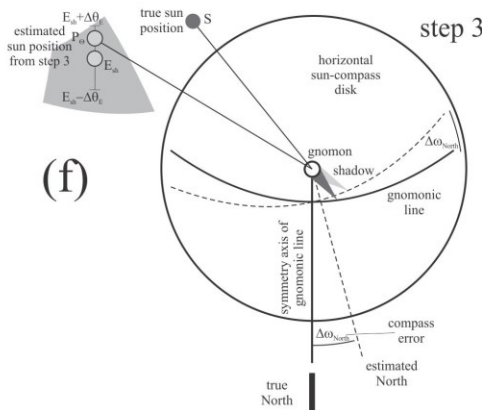
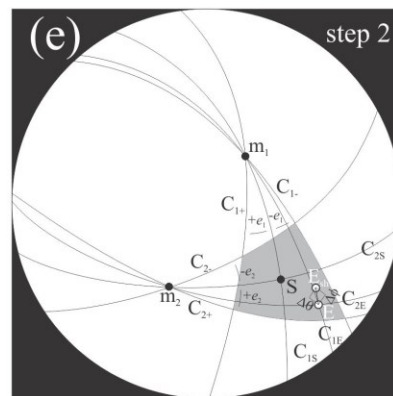
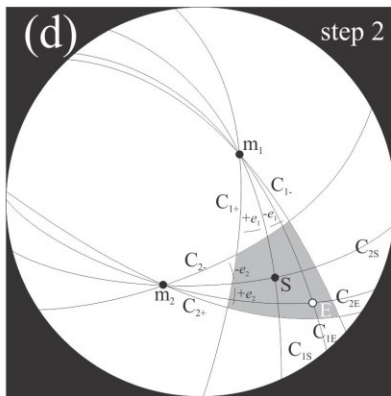
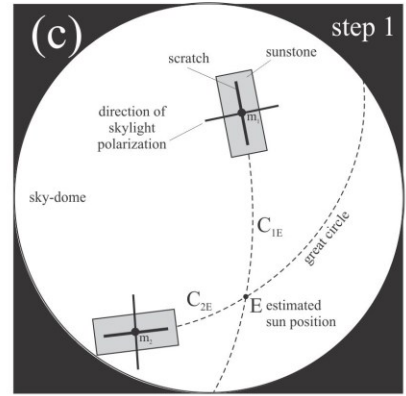
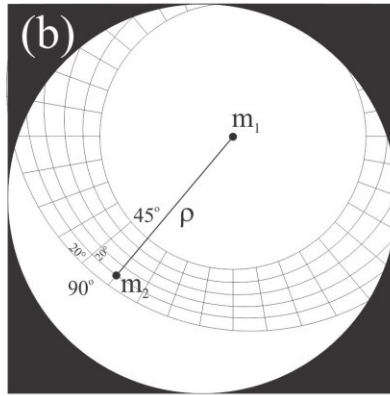
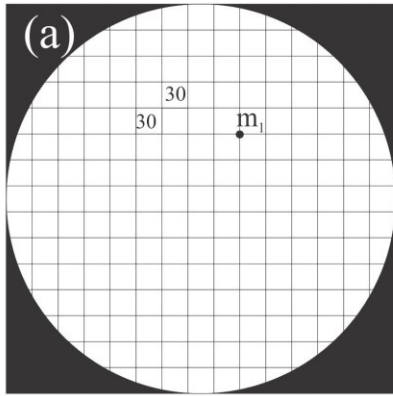


Figure 1: Steps of determination of the North uncertainty $\Delta\omega_N$. (a) Celestial square grid from which sky point m_1 is chosen, where the first sunstone is rotated. (b) Polar grid from which point m_2 is chosen, where the second sunstone is rotated at an angular distance γ from m_1 . (c) The 1st step of sky-polarimetric navigation. (d) Adjusting the orientation of sunstones at sky points m_1 and m_2 has uncertainties e_1 and e_2 , which determine a spherical rectangle (grey) containing the real Sun position S and all possible estimated Sun positions E . (e) By finding the intersection of the great celestial circles where the estimated Sun positions E are located, the navigator commits elevation uncertainty $\Delta\theta$ and azimuth uncertainty $\Delta\phi$, thus E has to be shifted with a vector of $(\Delta\theta, \Delta\phi)$ getting the shifted estimated Sun position E_{sh} . (f) The 3rd step of sky-polarimetric navigation with a North uncertainty $\Delta\omega_N$. The elevation of the Sun is estimated with an elevation uncertainty $\Delta\theta_E$, thus the estimated Sun position P_θ from step 3 can be found in the inaccuracy interval of $E_{sh} - \Delta\theta_E$ and $E_{sh} + \Delta\theta_E$. (g) In the 4th step, the navigator had to align the shadow-stick of the sun-compass parallel to the meridian (vertical azimuth plane) of the invisible Sun. The uncertainty of this alignment was characterized by the measured $e_{4th}(\theta)$ function and for each Sun position P_θ we got an interval between $\phi_S(\theta) - e_{4th}(\theta)$ and $\phi_S(\theta) + e_{4th}(\theta)$ that was divided into equal horizontal angular distances by 0.2° perpendicular to the meridian, where $\phi_S(\theta)$ is the azimuth angle of point P_θ . Thus the measured Sun position P_E , can be found in this inaccuracy interval. (h) Distribution (frequency f) of the North uncertainty $\Delta\omega_N$ with a maximum at angle ω_{max} and half bandwidth δ_ω being the full width at half maximum. (i) The two possibilities to project the estimated sun position E onto the forenoon and afternoon half of the gnomonic line. (j) The gnomonic lines for the spring equinox (21 March) and the summer solstice (21 June), onto which the real and estimated sun positions were projected. The angular deviation from the gnomonic lines gives the navigation uncertainty. G : gnomon. S_E : real sun position projected onto the equinoctial line. S'_E : estimated erroneous sun position projected onto the equinoctial line. P_E : point that we get after rotating S'_E to fit onto the equinoctial line (the main step of North uncertainty computation). S_S : real sun position projected onto the solstice line. S'_S : estimated erroneous sun position projected onto the solstice line. P_S : point that we get after rotating S'_S to fit onto the solstice line (the main step of North uncertainty computation). Grey: angles $\Delta\omega_N$ with which S'_E and S'_S need to be rotated to fit onto the equinoctial and solstice line, respectively. More details can be read in the text.

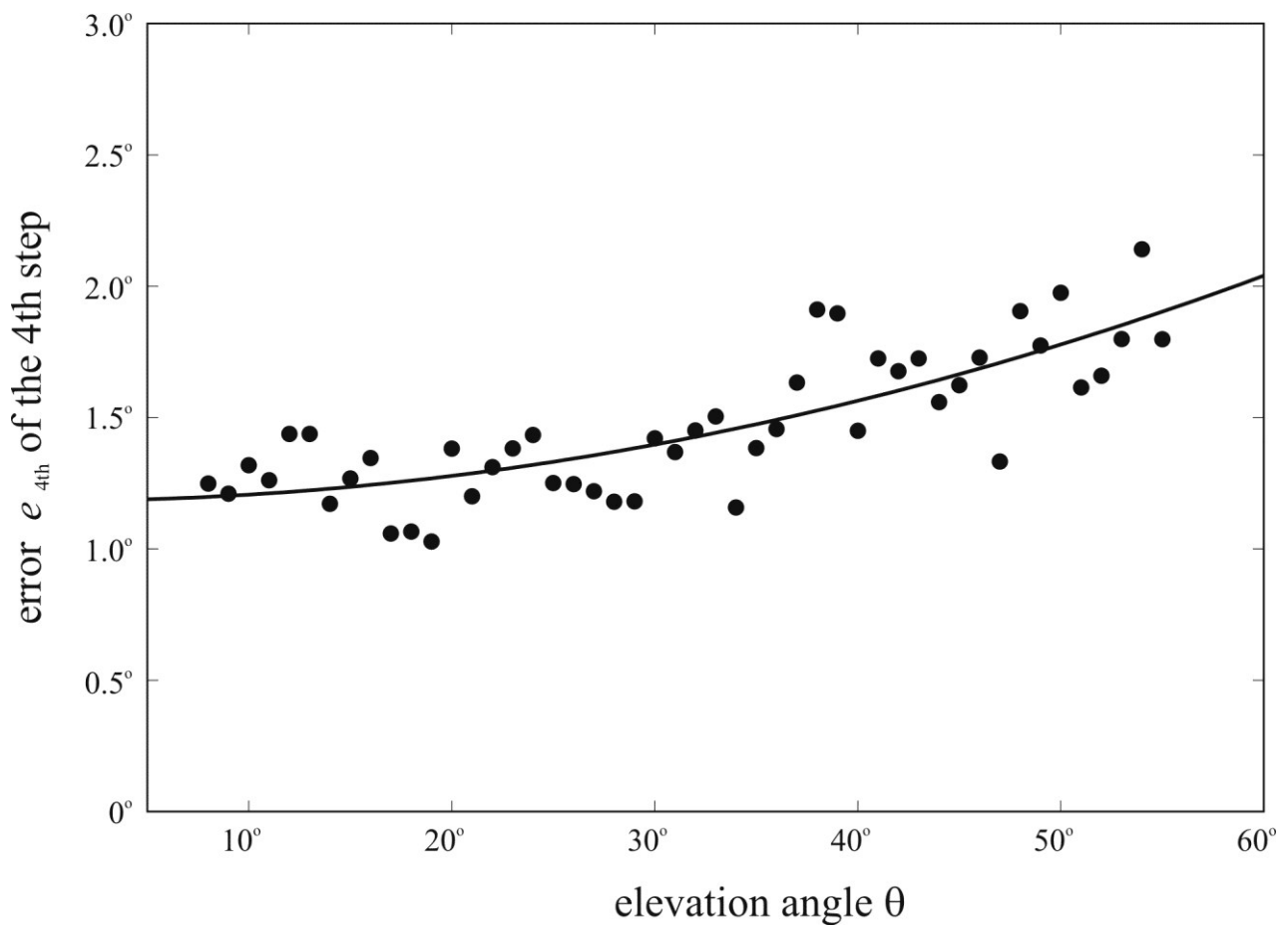


Figure 2: Uncertainty function $e_{4th}(\theta)$ of the 4th step of sky-polarimetric navigation. The continuous curve is the parabola fitted to the measured $e(\theta)$ -values.

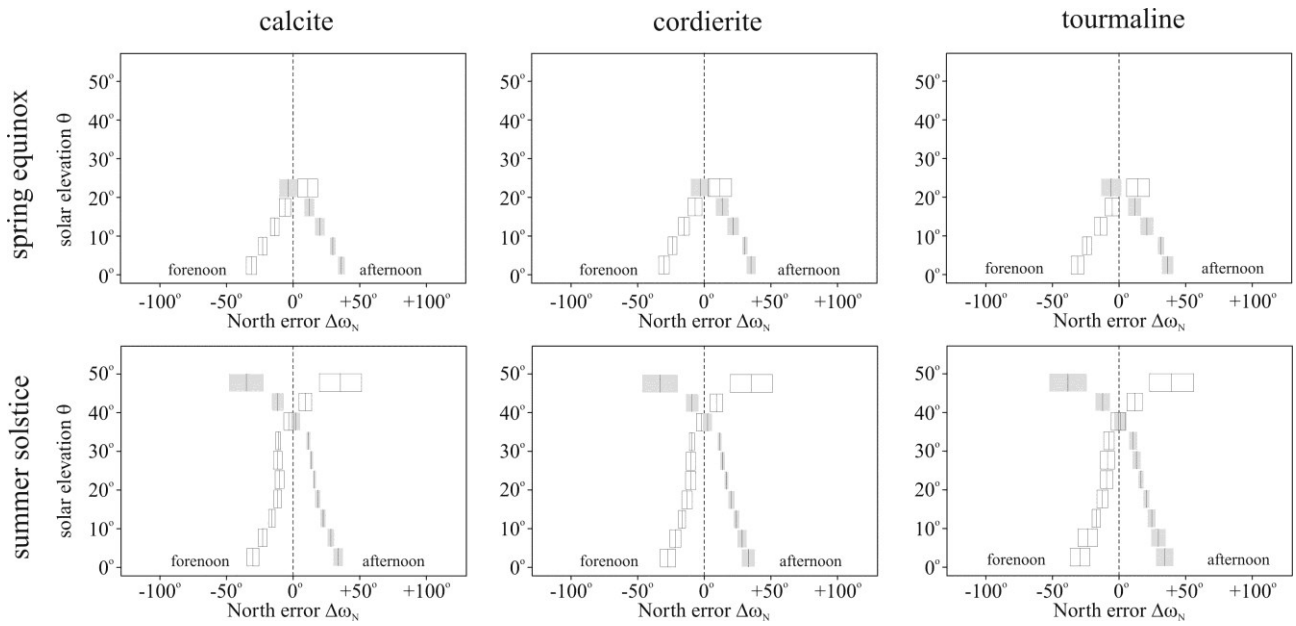


Figure 3: Weighted mean $\langle\omega_{\max}\rangle$ and standard deviation $\Delta\omega_{\max}$ of peaks ω_{\max} of North uncertainties (errors) for each elevation interval marked with rectangles for the calcite, cordierite and tourmaline sunstone crystals for navigation in the forenoon and afternoon at spring equinox and summer solstice. The horizontal length of rectangles is $2\Delta\omega_{\max}$ and the $\langle\omega_{\max}\rangle$ -values are shown by the vertical bars in the centers of the rectangles. White and grey rectangles mean data for forenoon and afternoon, respectively. The numerical values of these visualized data are in Supplementary Tables S1 (calcite), S2 (cordierite) and S3 (tourmaline). The vertical dashed line is at $\Delta\omega_N = 0^\circ$.

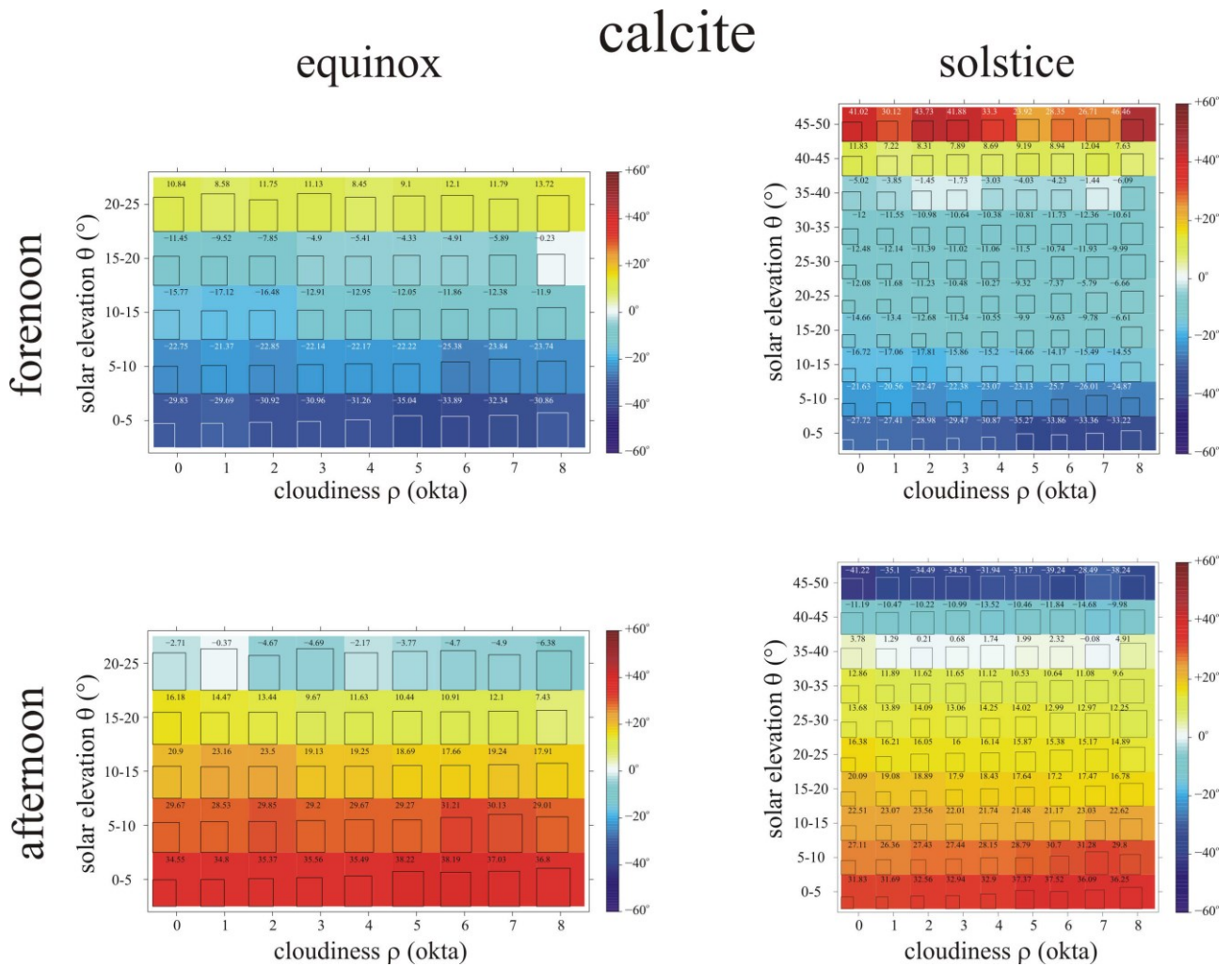


Figure 4: Colour matrix plot for calcite sunstone crystal where each cell belongs to a given solar elevation-cloudiness (θ , ρ) pair and contains the weighted mean $\langle\omega_{\max}\rangle$ of North uncertainties, the values of which are marked with a continuous colour transition from blue to red (blue meaning negative, red meaning positive values), and the relative standard error $\delta\omega_{\max}/(\delta\omega_{\max})_{\max}$ in the given dataset is marked with squares in the cell, the side length of which is proportional to the $\delta\omega_{\max}$ -values. The data for forenoon and afternoon navigation at spring equinox and summer solstice were visualized separately. The numerical values of these data are in Supplementary Table S4.

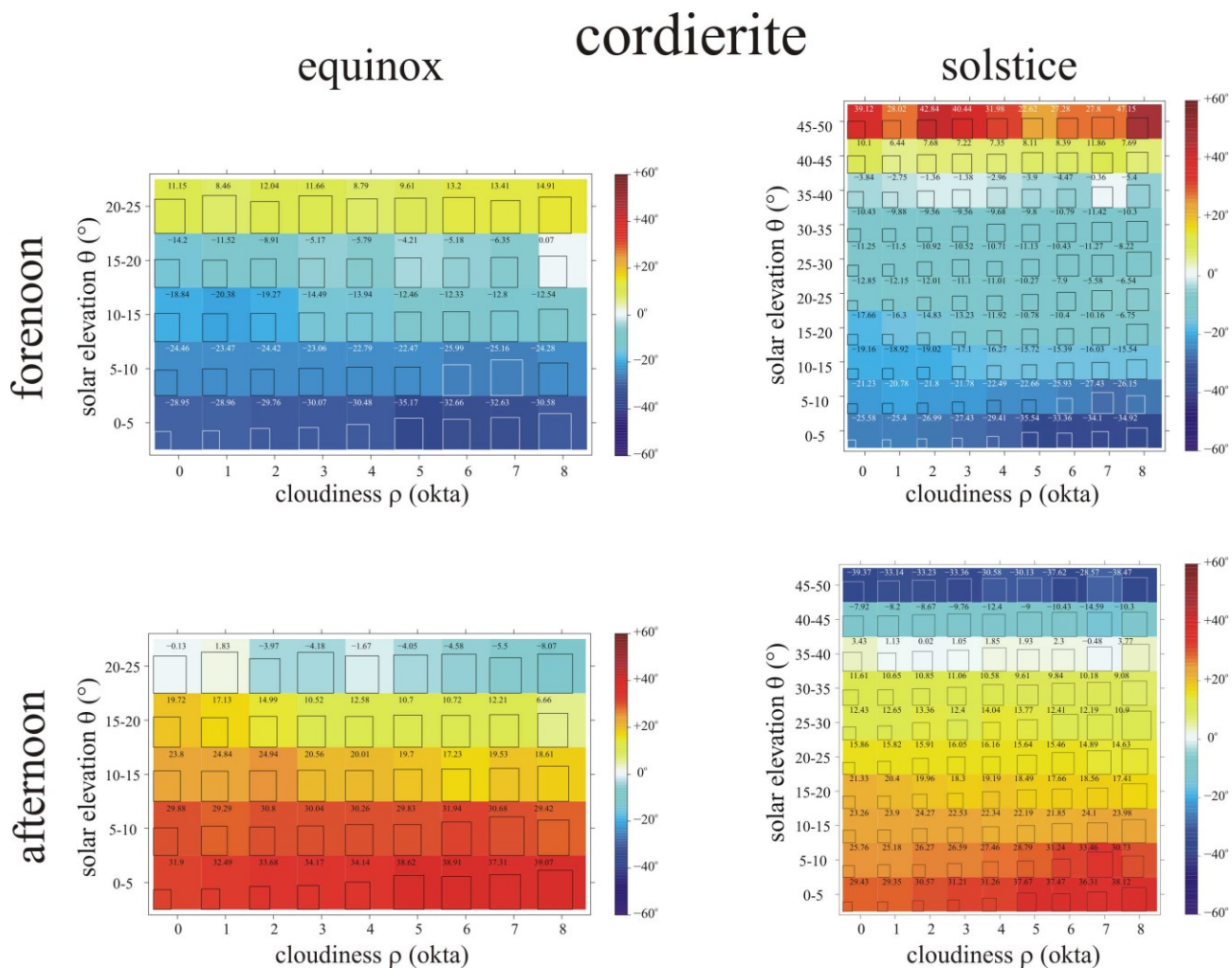


Figure 5: The same as Fig. 4 for cordierite sunstone crystal. The numerical values of these data are in Supplementary Table S5.

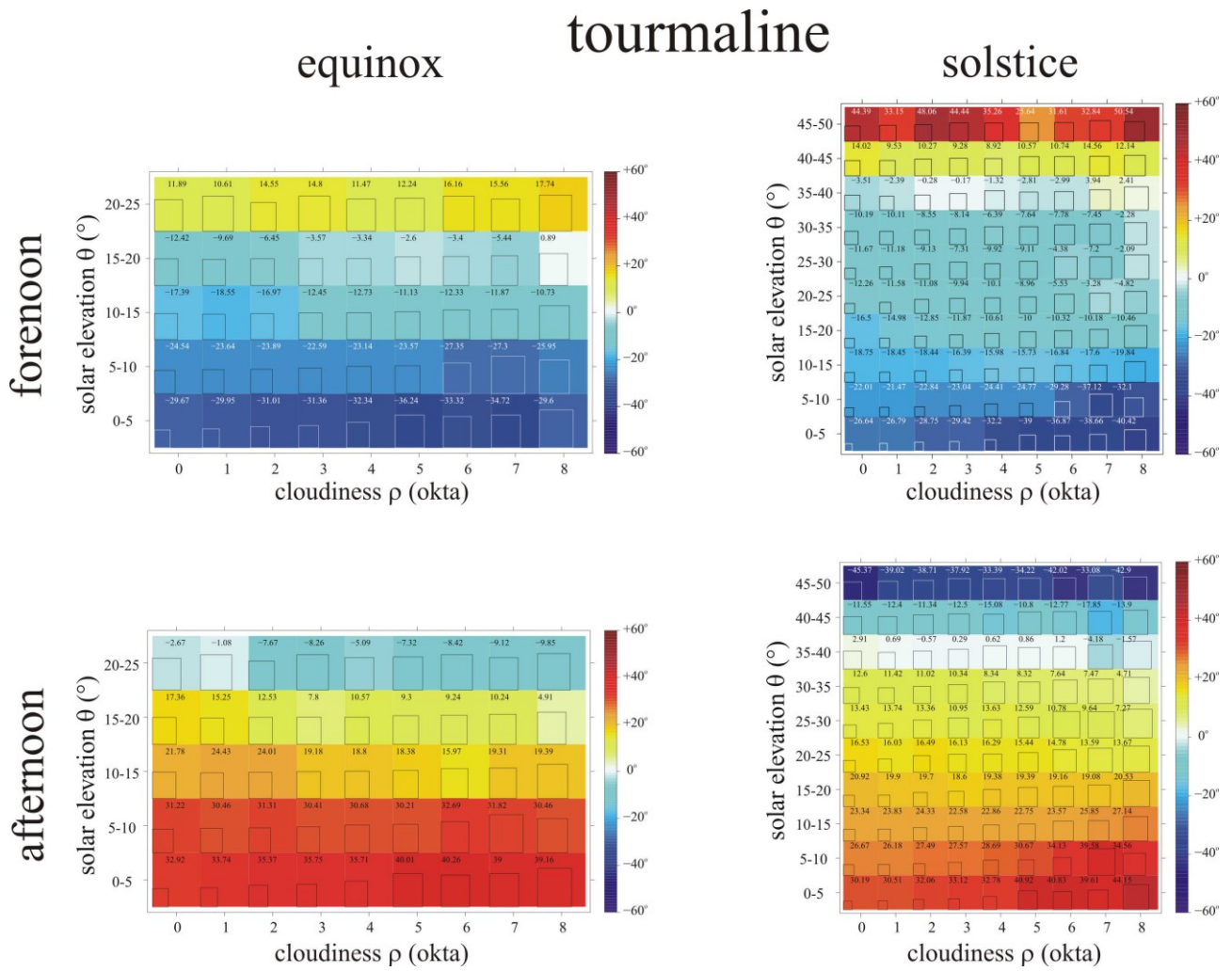


Figure 6: The same as Fig. 4 for tourmaline sunstone crystal. The numerical values of these data are in Supplementary Table S6.